Journal of Nuclear Medicine, published on December 29, 2022 as doi:10.2967/jnumed.122.264689

Fibroblast activation protein positron emission tomography and histopathology in a single-center database of 324 patients and 21 tumor entities

Running title

FAPI PET for Oncologic Imaging

Authors

Nader Hirmas[1], Rainer Hamacher[2], Miriam Sraieb[1], Marc Ingenwerth[3], Lukas Kessler[1], Kim M. Pabst[1], Francesco Barbato[1], Katharina Lueckerath[1], Stefan Kasper[2], Michael Nader[1], Hans-Ulrich Schildhaus[3,4], Claudia Kesch[5], Bastian von Tresckow[6], Christine Hanoun[6], Hubertus Hautzel[1], Clemens Aigner[7], Martin Glas[8], Martin Stuschke[9], Sherko Kümmel[10], Philipp Harter[11], Celine Lugnier[12], Waldemar Uhl[13], Marco Niedergethmann[14], Boris Hadaschik[5], Viktor Grünwald[5], Jens T. Siveke[15,16], Ken Herrmann[1], Wolfgang P. Fendler[1]

Affiliations

[1] Department of Nuclear Medicine, University of Duisburg-Essen and German Cancer Consortium (DKTK)-University Hospital Essen, Essen, Germany
[2] Department of Medical Oncology, West German Cancer Center, University of Duisburg-Essen and German Cancer Consortium (DKTK)-University Hospital Essen, Essen, Germany
[3] Institute of Pathology, University Hospital Essen, Essen, Germany
[4] Targos Molecular Pathology Inc., Kassel, Germany
[5] Department of Urology, University of Duisburg-Essen and German Cancer Consortium (DKTK)-University Hospital Essen, Essen, Germany
[6] Department of Hematology and Stem Cell Transplantation, University of Duisburg-

Essen and German Cancer Consortium (DKTK)-University Hospital Essen, Essen, Germany
[7] Department of Thoracic Surgery and Thoracic Endoscopy, University of Duisburg-Essen and German Cancer Consortium (DKTK)-University Hospital Essen, Essen, Germany
[8] Division of Clinical Neurooncology, Department of Neurology, University of Duisburg-Essen and German Cancer Consortium (DKTK)-University Hospital Essen, Essen, Germany
[9] Department of Radiation Therapy, University of Duisburg-Essen and German Cancer Consortium (DKTK)-University Hospital Essen, Essen, Germany
[10] Breast Unit, Kliniken Essen-Mitte, Essen, Germany, Charité – Universitätsmedizin Berlin, Department of Gynecology with Breast Center, Berlin, Germany
[11] Department of Gynecology and Gynecologic Oncology, Ev. Kliniken Essen-Mitte (KEM), Essen, Germany
[12] Department of Hematology and Oncology with Palliative Care, Ruhr-University Bochum, Bochum, Germany
[13] Department of General and Visceral Surgery, Ruhr-University Bochum, Bochum, Germany
[14] Clinic for General and Visceral Surgery, Alfried Krupp Hospital, Essen, Germany
[15] Bridge Institute of Experimental Tumor Therapy, West German Cancer Center, University Hospital Essen, Essen, Germany
[16] Division of Solid Tumor Translational Oncology, German Cancer Consortium (DKTK, Partner Site Essen) and German Cancer Research Center, DKFZ, Heidelberg, Germany

Corresponding author

Name: Wolfgang P. Fendler, MD

Address: Hufelandstraße 55, 45147 Essen, Germany

Tel.: +49 201 723 2032

Fax: +49 201 723 5658

E-mail: wolfgang.fendler@uk-essen.de

First author

Name: Nader Hirmas, MD

Position: Doctoral candidate

Address: Hufelandstraße 55, 45147 Essen, Germany

Tel.: +49 201 723 2032

Fax: +49 201 723 5658

E-mail: nader.hirmas@stud.uni-due.de

Word count

4,663 words.

Financial support

None.

ABSTRACT

Rationale: We present an overview of our prospective fibroblast activation protein inhibitors (FAPI) registry study across a 3-year period, with head-to-head comparison of tumor uptake in ^{68}Ga-FAPI and ^{18}F-FDG PET, as well as FAP immunohistochemistry.

Methods: This is an interim analysis of the ongoing ^{68}Ga-FAPI PET prospective observational trial at our Department. Patients who underwent clinical imaging with ^{68}Ga-FAPI PET between October 2018 and October 2021 were included. Tracer uptake for tumor lesions was quantified by SUV_{max} and for normal organs by SUV_{mean}. PET tumor volume (40% isocontour) and tumor-to-background ratios (TBR) were calculated. Correlation between SUV_{max} and FAP staining in tissue samples was analyzed.

Results: 324 patients with 21 different tumor entities underwent ^{68}Ga-FAPI imaging; 237 patients additionally received ^{18}F-FDG PET. The most common tumor entities were sarcoma (131/324, 40%), pancreatic carcinoma (67/324, 21%), and primary tumors of the brain (22/324, 7%). Mean primary tumor SUV_{max} was significantly higher for ^{68}Ga-FAPI than ^{18}F-FDG among pancreatic cancers (13.2 vs. 6.1, $p<0.001$) and sarcoma (14.3 vs. 9.4, $p<0.001$), and the same was true for mean SUV_{max} in metastatic lesions of pancreatic cancers (9.4 vs. 5.5, $p<0.001$). Mean primary tumor TBR_{max} was significantly higher for ^{68}Ga-FAPI than ^{18}F-FDG across several tumor entities, most prominently pancreatic cancers (14.7 vs. 3.0, $p<0.001$) and sarcoma (17.3 vs. 4.7, $p<0.001$). Compared to ^{18}F-FDG, ^{68}Ga-FAPI showed superior detection for locoregional disease in sarcoma (52 vs. 48 total regions detected) as well as for distant metastatic disease in both, sarcoma (137 vs. 131) and pancreatic cancer (65 vs. 57), respectively. Among 61 histopathology

samples, there was a positive correlation between ^{68}Ga-FAPI SUV_{max} and overall FAP immunohistochemistry score (r=0.352, p=0.005).

Conclusion: ^{68}Ga-FAPI demonstrates higher absolute uptake in pancreatic cancers and sarcoma, as well as higher tumor-to-background uptake along with improved tumor detection for pancreatic cancers, sarcoma, and other tumor entities when compared to ^{18}F-FDG. ^{68}Ga-FAPI is a new tool for tumor staging with theranostic potential.

Keywords

FAPI; PET; oncology; staging; theranostic.

INTRODUCTION

Imaging is critically important in the diagnosis and staging of malignancies, with varying detection rates depending on the tumor entity and diagnostic modality. Positron emission tomography (PET) of cancer cells using fluorodeoxyglucose (^{18}F-FDG) PET acquires additional molecular information useful for the management of disease and for improving treatment outcomes (*1-3*).

Tumor growth and spread are not only determined by cancer cells, but also by the tumor microenvironment, which contains several nonmalignant components. Besides immune cells, important constituents are cancer-associated fibroblasts, which are known to be involved in tumor growth, migration, and progression (*4*). Although heterogeneous in their origin, cancer-associated fibroblasts have common properties which are distinct from normal fibroblasts, expressing proteins not found in their normal counterparts (*5*). A subpopulation of cancer-associated fibroblasts expresses fibroblast activation protein alpha (FAPα), among other markers, which is associated with pro-tumorigenic functions (*6-10*).

Therefore, these cells represent attractive diagnostic and therapeutic targets. Since 2018, preclinical and clinical data have emerged on a variety of FAP-directed therapies, including radiolabeled, low-molecular weight FAP inhibitors (FAPIs), further underlining their favorable properties in diagnosis and therapy (*11-15*).

Data for the superiority of ^{68}Ga-FAPI PET over conventional imaging have been reported previously in small cohorts (*13,16*). Based on its favorable imaging characteristics, patients were referred for clinical ^{68}Ga-FAPI PET staging, both at initial diagnosis and post-intervention, and offered enrollment in our prospective observational

^{68}Ga-FAPI registry. Clinical indications for ^{68}Ga-FAPI PET were staging of high-risk patients, evaluation of the localization of tumor lesions before biopsy or surgery, equivocal imaging results, or evaluation of therapeutic options.

In this report, we present the largest cohort to date, with an overview of the tumor entities diagnosed and staged with ^{68}Ga-FAPI across a 3-year period, including head-to-head comparison of tumor uptake in ^{68}Ga-FAPI and ^{18}F-FDG PET, as well as FAP immunohistochemistry.

MATERIALS AND METHODS

Study design and participants

Patients underwent imaging with ^{68}Ga-FAPI PET between October 2018 and October 2021 at the Department of Nuclear Medicine at the University Hospital Essen. This is an interim analysis of the ongoing ^{68}Ga-FAPI PET observational trial conducted at the University Hospital Essen (NCT04571086). Until October 2021, adult patients who underwent clinical ^{68}Ga-FAPI PET were offered the possibility to consent to a prospective observational trial for correlation and clinical follow-up of PET findings. Evaluation of data was approved by the ethics committee of the University Duisburg-Essen (20-9485-BO and 19-8991-BO). Patient subgroups have been reported in previous publications (N=47 (*17*), N=69 (*18*), and N=91 (*19*)).

Details of data collection (*20-22*), imaging and administration of radioligands (*18,23,24*), imaging analysis, immunohistochemistry and FAP scoring (*17,25*), as well as statistical analysis (*26*) are provided in the Supplemental Material.

RESULTS

Patient Characteristics

Three hundred and twenty-four patients were included; patient characteristics are outlined in Table 1. The median age was 59 years (IQR: 16). The most common tumor entities were sarcoma (131/324, 40%), followed by primary tumors of the pancreas (67/324, 21%), brain (22/324, 7%), lung (14/324, 4%), and pleural mesothelioma (12/324, 4%). The majority of patients (235/324, 73%) underwent ^{68}Ga-FAPI PET imaging for restaging purposes. A breakdown of histopathological diagnoses as well as presence of primary and metastatic lesions for each category is provided in Supplemental Table 1.

Tumor diagnostics and ^{68}Ga-FAPI PET

The mean SUV_{max} for primary lesions and metastatic lesions on ^{68}Ga-FAPI PET are shown in Fig. 1A and 1B, respectively. Mean values of primary tumor SUV_{max} range from 3.41 for brain tumors to 21.44 for ovarian tumors. Mean primary tumor SUV_{max} was higher than 10 for 9/17 (53%) of tumor entities with primary lesions, including prostate (10.4), bladder (10.5), pancreas (13.2), and sarcoma (14.1), among others. Mean SUV_{max} for primary lesions and metastatic lesions using broader subgroups are provided in Supplemental Fig. 1.

Staging by ^{68}Ga-FAPI PET is presented in Supplemental Fig. 2 for the seven most common tumor entities in our registry (with at least ten patients, excluding brain tumors). In our prospective cohort, distant metastatic disease was detected in the majority of patients with carcinomas of the head and neck (8/9, 89%) and pancreas (44/67, 66%), sarcoma (79/122, 65%), carcinomas of the colon/rectum (7/11, 64%), prostate (7/11,

64%), and bladder (5/8, 63%), and cholangiocellular carcinoma (CCC, 6/11, 55%). Loco-regional only disease was detected most often in carcinomas of the lung (11/14, 79%) and pleural mesothelioma (9/12, 75%).

^{68}Ga-FAPI PET vs. ^{18}F-FDG PET Imaging

In our cohort, 237/324 of patients (73%) had undergone additional ^{18}F-FDG PET, and a head-to-head analysis of both imaging modalities was performed. Mean SUV_{max} was significantly higher for ^{68}Ga-FAPI than ^{18}F-FDG PET among primary tumors of the pancreas (13.2 vs. 6.1, $p<0.001$) and sarcoma (14.3 vs. 9.4, $p<0.001$), as shown in Fig. 2A. Similarly, the mean SUV_{max} in metastatic lesions was significantly higher for ^{68}Ga-FAPI than ^{18}F-FDG in pancreatic cancer (9.4 vs. 5.5, $p<0.001$, Fig. 2B).

For primary tumors, mean TBR_{max} (with blood pool background) was significantly higher for ^{68}Ga-FAPI than ^{18}F-FDG in pancreatic cancer (9.9 vs. 3.5, $p<0.001$) and sarcoma (10.4 vs. 5.8, $p<0.001$) as shown in Fig. 3A. Mean TBR_{max} (with liver background) was also significantly higher for ^{68}Ga-FAPI than ^{18}F-FDG in pancreatic cancer (14.7 vs. 3.0, $p<0.001$) and sarcoma (17.3 vs. 4.7, $p<0.001$), in addition to prostate cancer (7.8 vs. 2.7, $p=0.017$), pleural mesothelioma (12.9 vs. 5.0, $p=0.003$), head and neck cancer (14.5 vs. 4.2, $p=0.013$), and CCC (19.5 vs. 3.6, $p=0.016$), as shown in Fig. 3B. Conversely, mean TBR_{max} (with muscle background) was significantly lower for ^{68}Ga-FAPI than ^{18}F-FDG in pleural mesothelioma (9.4 vs. 17.6, $p=0.004$, Fig. 3C).

For metastatic lesions, mean TBR_{max} (with blood pool background) was significantly higher for ^{68}Ga-FAPI than ^{18}F-FDG in pancreatic cancer (7.0 vs. 3.4, $p<0.001$) and sarcoma (9.8 vs. 5.8, $p=0.028$) as shown in Fig. 4A. Mean TBR_{max} (with

liver background) was also significantly higher for ^{68}Ga-FAPI than ^{18}F-FDG for pancreatic cancer (10.6 vs. 2.8, p<0.001) and sarcoma (18.9 vs. 4.7, p=0.003), in addition to prostate cancer (15.1 vs. 4.9, p<0.001), pleural mesothelioma (13.5 vs. 4.8, p=0.017), and CCC (14.5 vs. 3.9, p=0.012), as shown in Fig. 4B. Conversely, mean TBR_{max} (with muscle background) was significantly lower for ^{68}Ga-FAPI than ^{18}F-FDG in pleural mesothelioma (9.4 vs. 17.8, p=0.027), prostate cancer (8.0 vs. 15.6, p=0.009), and CCC (10.0 vs. 15.4, p=0.024), as shown in Fig. 4C.

There were no significant differences between metabolic tumor volumes measured for primary lesions and metastatic lesions in ^{68}Ga-FAPI and ^{18}F-FDG PET scans across tumor entities, as shown in Supplemental Fig. 3.

Examples of ^{68}Ga-FAPI and ^{18}F-FDG PET scans of patients showing tumor uptakes and FAPα stain in tumor samples are presented in Supplemental Fig. 4-8.

A comparison of primary SUV_{max} and involved regions between ^{68}Ga-FAPI and ^{18}F-FDG PET among metastatic and non-metastatic disease and across tumor entities is provided in Supplemental Table 2. When compared to ^{18}F-FDG, ^{68}Ga-FAPI showed superior detection for locoregional disease in sarcoma (52 vs. 48 total regions detected) as well as for distant metastatic disease in sarcoma (137 vs. 131) and cancers of the pancreas (65 vs. 57), head and neck (15 vs. 13), CCC (12 vs. 11), lung (9 vs. 8), and bladder (8 vs. 7), respectively. However, ^{68}Ga-FAPI showed inferior detection of lymphoma compared to ^{18}F-FDG (7 vs. 10), respectively.

Immunohistochemistry and FAP Scoring

Sixty-one tissue samples dated within 3 months from the date of ^{68}Ga-FAPI PET (median 20.5 days, IQR 23 days) were analyzed and scored (sarcoma N=33, pancreas N=11, pleura N=5, urothelial N=4, colorectal N=3, head and neck N=3, prostate N=1, and lung N=1). The corresponding SUV_{max} on ^{68}Ga-FAPI PET measured for the specific lesions biopsied before or after ^{68}Ga-FAPI PET, or surgically removed after ^{68}Ga-FAPI PET, were included in the correlation analysis. Across the 61 samples, there was a significant positive correlation between the overall score for FAPα immunohistochemistry and ^{68}Ga-FAPI SUV_{max} (r=0.352, p=0.005, Fig. 5).

DISCUSSION

We report findings for 324 patients with 21 tumor entities diagnosed and staged by ^{68}Ga-FAPI PET as part of our registry study over a three-year period with a head-to-head analysis of ^{68}Ga-FAPI versus ^{18}F-FDG PET uptake in tumor and metastatic lesions as well as correlation between ^{68}Ga-FAPI uptake and FAPα expression in tissue samples. This represents the largest cohort of patients examined with this novel imaging modality. Our results demonstrate higher tumor-to-liver uptake ratios for ^{68}Ga-FAPI as compared to ^{18}F-FDG for 6/14 (43%) of the evaluated tumor entities (most prominently sarcoma and pancreatic cancer, in addition to head and neck cancer, prostate cancer, CCC, and pleural mesothelioma) and comparable results in 8/14 (57%). Furthermore, we observed a positive correlation between radiotracer uptake and FAPα immunohistochemistry staining.

Relatively low ^{68}Ga-FAPI uptake in normal parenchyma improves tumor

delineation, especially in regions with high physiologic glucose uptake. Thus, ^{68}Ga-FAPI demonstrates improved per-region tumor detection for pancreatic cancers, sarcoma, CCC, prostate cancer, pleural mesothelioma, and head and neck cancer when compared to ^{18}F-FDG. As such, ^{68}Ga-FAPI PET is a promising imaging modality for these entities, and it has the potential for more precise staging and management of patients as well as theranostic screening.

^{68}Ga-FAPI PET images the protein FAPα, which is primarily located on CAFs in the stroma, but this protein can also be found on tumor cells. High tumor and low organ uptakes support the potential use of FAPI ligands in a therapeutic context, particularly for sarcoma and pancreatic cancer. Feasibility of FAP-directed radioligand therapy has been reported for breast (*11*) and ovarian cancer (*27*), sarcoma and pancreatic cancers (*15,28*), as well as multiple advanced and refractory tumors (*14,29,30*). All applications of FAP-directed radioligand therapy relied on baseline patient selection by high uptake on ^{68}Ga-FAPI PET. In addition, FAP-targeting drugs have been showing clinical promise across various tumor entities; one prominent example is talabostat, which has shown tumor control in 21% of patients with colorectal cancer (*31*). As such, future drug developments and their potential clinical applications may be enhanced through ^{68}Ga-FAPI imaging, which aids in selecting patients whose tumors exhibit high ^{68}Ga-FAPI uptake and low glycolytic phenotypes, and who would potentially benefit from FAP-directed radioligand therapy.

Another ongoing clinical trial at our department (NCT05160051) aims to explore the diagnostic accuracy of ^{68}Ga-FAPI-46 PET as well as its impact on management and inter-reader reproducibility for different FAP-expressing tumor entities. Here, tumor

samples will be collected within 8 weeks from the time of the ^{68}Ga-FAPI PET scan to better elucidate the correlation between ^{68}Ga-FAPI-46 uptake intensity and histopathologic FAP expression.

Our analysis has several limitations. SUV for ^{68}Ga-FAPI is reproducible at different time-points (*18*) and routinely measured but not yet a well-established metric. In addition, for some patient subgroups, there were low sample sizes as well as referral bias. We report SUV values from different PET devices; despite cross calibration based on EARL standards, SUV deviations may have occurred but were not significantly different (e.g., random samples with equal numbers of patients, p=0.949). Moreover, quantitative immunohistochemistry assessment across all plains of whole mount pathology specimens was not feasible, which may have led to deviations between ^{68}Ga-FAPI SUV_{max} and immunohistochemistry scores.

CONCLUSION

In summary, ^{68}Ga-FAPI demonstrates higher absolute uptake in pancreatic cancers and sarcoma, as well as higher tumor-to-background uptake along with improved tumor detection for pancreatic cancers, sarcoma, CCC, prostate cancer, pleural mesothelioma, and head and neck cancer when compared to ^{18}F-FDG. A prospective clinical trial at our department (NCT05160051) is currently underway.

Financial Disclosure

Rainer Hamacher is supported by Clinician Scientist Program of the University Medicine Essen Clinician Scientist Academy (UMEA) sponsored by faculty of medicine and Deutsche Forschungsgemeinschaft (DFG) and has received travel grants from Lilly, Novartis, and Pharma Mar, as well as fees from Lilly and Pharma Mar. Lukas Kessler is a consultant for AAA and BTG and received fees from Sanofi. Kim M. Pabst has received a Junior Clinician Scientist Stipend of the University Medicine Essen Clinician Scientist Academy (UMEA) sponsored by the Faculty of Medicine at the University of Duisburg-Essen and the Deutsche Forschungsgemeinschaft (DFG), and he has received research funding from Bayer outside of the submitted work. Katharina Lueckerath is a consultant for Sofie Biosciences and receives research funding from Curie Therapeutics. Stefan Kasper reports personal fees and grants from AstraZeneca, Merck Serone, Merck Sharpe & Dohme, Amgen, Bristol Myers Squibb, Roche, Lilly, Servier, Incyte, and SanofiAventis outside of the submitted work. Claudia Kesch has received consultant fees from Apogepha, research funding from AAA/Novartis and Curie Therapeutics, and compensation for travel from Janssen R&D. Bastian von Tresckow is an advisor or consultant for Allogene, BMS/Celgene, Cerus, Incyte, Miltenyi, Novartis, Pentixafarm, Roche, Amgen, Pfizer, Takeda, Merck Sharp & Dohme, and Gilead Kite, has received honoraria from AstraZeneca, Novartis, Roche Pharma AG, Takeda, and Merck Sharp & Dohme, reports research funding from Novartis (Inst), Merck Sharp & Dohme (Inst), and Takeda (Inst), and reports travel support from AbbVie, AstraZeneca, Kite-Gilead, Merck Sharp & Dohme, Takeda, and Novartis. Christine Hanoun received honoraria from BMS, TAKEDA, and AstraZeneca, travel grants from AbbVie, and research funding from

Novartis. Hubertus Hautzel reports research funding and travel support from PARI GmbH outside of the submitted work. Ken Herrmann reports personal fees from Bayer, SIRTEX, Adacap, Curium, Endocyte, IPSEN, Siemens Healthineers, GE Healthcare, Amgen, Novartis, ymabs, Aktis, Oncology, and Pharma15, as well as personal and other fees from Sofie Biosciences, non-financial support from ABX, and grants and personal fees from BTG, all of which are outside of the submitted work. Boris Hadaschik has had advisory roles for ABX, AAA/Novartis, Astellas, AstraZeneca, Bayer, Bristol Myers Squibb, Janssen R&D, Lightpoint Medical, Inc., and Pfizer, has received research funding from Astellas, Bristol Myers Squibb, AAA/Novartis, German Research Foundation, Janssen R&D, and Pfizer, and has received compensation for travel from Astellas, AstraZeneca, Bayer, and Janssen R&D. Philipp Harter reports grants, personal fees and non-financial support from Astra Zeneca and GSK, grants and personal fees from Roche, MSD, Clovis, and Immunogen, personal fees from Mersana, Sotio, Stryker, and Zai Lab, grants from Boehringer Ingelheim, Medac, Genmab, Deutsche Krebshilfe, Deutsche Forschungsgemeinschaft, and the European Union, all of which are outside of the submitted work. Jens T. Siveke received honoraria as consultant or for continuing medical education presentations from AstraZeneca, Bayer, Bristol-Myers Squibb, Eisbach Bio, Immunocore, Novartis, Roche/Genentech, and Servier, his institution receives research funding from Bristol-Myers Squibb, Celgene, Eisbach Bio, and Roche/Genentech, and he holds ownership and serves on the Board of Directors of Pharma15, all outside of the submitted work. Wolfgang P. Fendler reports fees from SOFIE Bioscience (research funding), Janssen (consultant, speakers' bureau), Calyx (consultant), Bayer (consultant, speakers' bureau, research funding), and Parexel (image

review) as well as financial support from Mercator Research Center Ruhr (MERCUR, An-2019-0001), IFORES (D/107-81260, D/107-30240), and Wiedenfeld-Stiftung/Stiftung Krebsforschung Duisburg, all outside of the submitted work. No other potential conflicts of interest relevant to this article exist.

KEY POINTS

QUESTION: What is the ^{68}Ga-FAPI PET uptake for different tumor entities?

PERTINENT FINDINGS: We report an overview of our FAPI registry including 324 patients with 21 tumor entities during a 3-year period, including staging findings as well as head-to-head analysis of ^{68}Ga-FAPI versus ^{18}F-FDG PET uptake in tumor lesions, and correlation between ^{68}Ga-FAPI uptake and FAP expression in tissue samples. Mean SUV_{max} was significantly higher for ^{68}Ga-FAPI than ^{18}F-FDG in primary lesions of pancreatic cancers and sarcoma, and in metastatic lesions of pancreatic cancers. The mean TBR_{max} in primary lesions was also superior for ^{68}Ga-FAPI than ^{18}F-FDG in sarcoma and cancers of the head and neck, prostate, CCC, pancreas, and pleura, and it was comparable for the remaining entities. In addition, we report a positive correlation between radiotracer uptake and FAP expression levels in tissue samples. Finally, when compared to ^{18}F-FDG, ^{68}Ga-FAPI showed superior detection for locoregional disease in sarcoma, as well as for distant metastatic disease in sarcoma and cancers of the pancreas, head and neck, CCC, lung, and bladder.

IMPLICATIONS FOR PATIENT CARE: ^{68}Ga-FAPI PET demonstrates high uptake and is particularly suited for imaging sarcoma and cancers of the head and neck, prostate, CCC, pancreas, and pleura. ^{68}Ga-FAPI PET offers theranostic screening and has the potential for more precise staging and management of patients with these entities.

REFERENCES

1. van Tinteren H, Hoekstra OS, Smit EF, et al. Effectiveness of positron emission tomography in the preoperative assessment of patients with suspected non-small-cell lung cancer: the PLUS multicentre randomised trial. *The Lancet.* 2002;359:1388-1392.

2. Ell PJ. The contribution of PET/CT to improved patient management. *Br J Radiol.* 2006;79:32-36.

3. Choi JY, Lee KH, Shim YM, et al. Improved detection of individual nodal involvement in squamous cell carcinoma of the esophagus by FDG PET. *J Nucl Med.* 2000;41:808-815.

4. Erdogan B, Ao M, White LM, et al. Cancer-associated fibroblasts promote directional cancer cell migration by aligning fibronectin. *J Cell Biol.* 2017;216:3799-3816.

5. Gascard P, Tlsty TD. Carcinoma-associated fibroblasts: orchestrating the composition of malignancy. *Genes Dev.* 2016;30:1002-1019.

6. Chen WT, Kelly T. Seprase complexes in cellular invasiveness. *Cancer Metastasis Rev.* 2003;22:259-269.

7. Keane FM, Nadvi NA, Yao TW, Gorrell MD. Neuropeptide Y, B-type natriuretic peptide, substance P and peptide YY are novel substrates of fibroblast activation protein-alpha. *FEBS J.* 2011;278:1316-1332.

8. Huang Y, Wang S, Kelly T. Seprase promotes rapid tumor growth and increased microvessel density in a mouse model of human breast cancer. *Cancer Res.* 2004;64:2712-2716.

9. Kelly T. Fibroblast activation protein-alpha and dipeptidyl peptidase IV (CD26): cell-surface proteases that activate cell signaling and are potential targets for cancer therapy. *Drug Resist Updat.* 2005;8:51-58.

10. Mueller SC, Ghersi G, Akiyama SK, et al. A novel protease-docking function of integrin at invadopodia. *J Biol Chem.* 1999;274:24947-24952.

11. Lindner T, Loktev A, Altmann A, et al. Development of quinoline-based theranostic ligands for the targeting of fibroblast activation protein. *J Nucl Med.* 2018;59:1415-1422.

12. Loktev A, Lindner T, Mier W, et al. A tumor-imaging method targeting cancer-associated fibroblasts. *J Nucl Med.* 2018;59:1423-1429.

13. Giesel FL, Kratochwil C, Lindner T, et al. (68)Ga-FAPI PET/CT: Biodistribution and preliminary dosimetry estimate of 2 DOTA-containing FAP-targeting agents in patients with various cancers. *J Nucl Med.* 2019;60:386-392.

14. Baum RP, Schuchardt C, Singh A, et al. Feasibility, biodistribution, and preliminary dosimetry in peptide-targeted radionuclide therapy of diverse adenocarcinomas using (177)Lu-FAP-2286: First-in-humans results. *J Nucl Med.* 2022;63:415-423.

15. Ferdinandus J, Fragoso Costa P, Kessler L, et al. Initial clinical experience with (90)Y-FAPI-46 radioligand therapy for advanced stage solid tumors: a case series of nine patients. *J Nucl Med.* 2022;63:727-734.

16. Kratochwil C, Flechsig P, Lindner T, et al. (68)Ga-FAPI PET/CT: Tracer uptake in 28 different kinds of cancer. *J Nucl Med.* 2019;60:801-805.

17. Kessler L, Ferdinandus J, Hirmas N, et al. (68)Ga-FAPI as a diagnostic tool in sarcoma: Data from the (68)Ga-FAPI PET prospective observational trial. *J Nucl Med.* 2022;63:89-95.

18. Ferdinandus J, Kessler L, Hirmas N, et al. Equivalent tumor detection for early and late FAPI-46 PET acquisition. *Eur J Nucl Med Mol Imaging.* 2021;48:3221-3227.

19. Kessler L, Ferdinandus J, Hirmas N, et al. Pitfalls and common findings in (68)Ga-FAPI-PET - A pictorial analysis. *J Nucl Med.* 2022;63:890-896.

20. Harris PA, Taylor R, Minor BL, et al. The REDCap consortium: Building an international community of software platform partners. *J Biomed Inform.* 2019;95:103208.

21. Harris PA, Taylor R, Thielke R, Payne J, Gonzalez N, Conde JG. Research electronic data capture (REDCap)--a metadata-driven methodology and workflow process for providing translational research informatics support. *J Biomed Inform.* 2009;42:377-381.

22. Amin MB, Edge S, Greene F, et al. *AJCC Cancer Staging Manual.* 8th ed. Springer International Publishing; 2017:55-986.

23. Lindner T, Loktev A, Giesel F, Kratochwil C, Altmann A, Haberkorn U. Targeting of activated fibroblasts for imaging and therapy. *EJNMMI Radiopharm Chem.* 2019;4:16.

24. Loktev A, Lindner T, Burger EM, et al. Development of fibroblast activation protein-targeted radiotracers with improved tumor retention. *J Nucl Med.* 2019;60:1421-1429.

25. Henry LR, Lee HO, Lee JS, et al. Clinical implications of fibroblast activation protein in patients with colon cancer. *Clin Cancer Res.* 2007;13:1736-1741.

26. Hinkle DE, Wiersma W, Jurs SG. *Applied Statistics for the Behavioral Sciences*. 2nd ed. Boston: Houghton Mifflin; 2003: 118.

27. Lindner T, Altmann A, Kramer S, et al. Design and development of (99m)Tc-labeled FAPI tracers for SPECT imaging and (188)Re therapy. *J Nucl Med.* 2020;61:1507-1513.

28. Kratochwil C, Giesel FL, Rathke H, et al. [(153)Sm]Samarium-labeled FAPI-46 radioligand therapy in a patient with lung metastases of a sarcoma. *Eur J Nucl Med Mol Imaging.* 2021;48:3011-3013.

29. Kuyumcu S, Kovan B, Sanli Y, et al. Safety of fibroblast activation protein-targeted radionuclide therapy by a low-dose dosimetric approach using 177Lu-FAPI04. *Clin Nucl Med.* 2021;46:641-646.

30. Assadi M, Rekabpour SJ, Jafari E, et al. Feasibility and therapeutic potential of 177Lu-fibroblast activation protein inhibitor-46 for patients with relapsed or refractory cancers: A preliminary study. *Clin Nucl Med.* 2021;46:e523-e530.

31. Narra K, Mullins SR, Lee HO, et al. Phase II trial of single agent Val-boroPro (Talabostat) inhibiting Fibroblast Activation Protein in patients with metastatic colorectal cancer. *Cancer Biol Ther.* 2007;6:1691-1699.

FIGURES

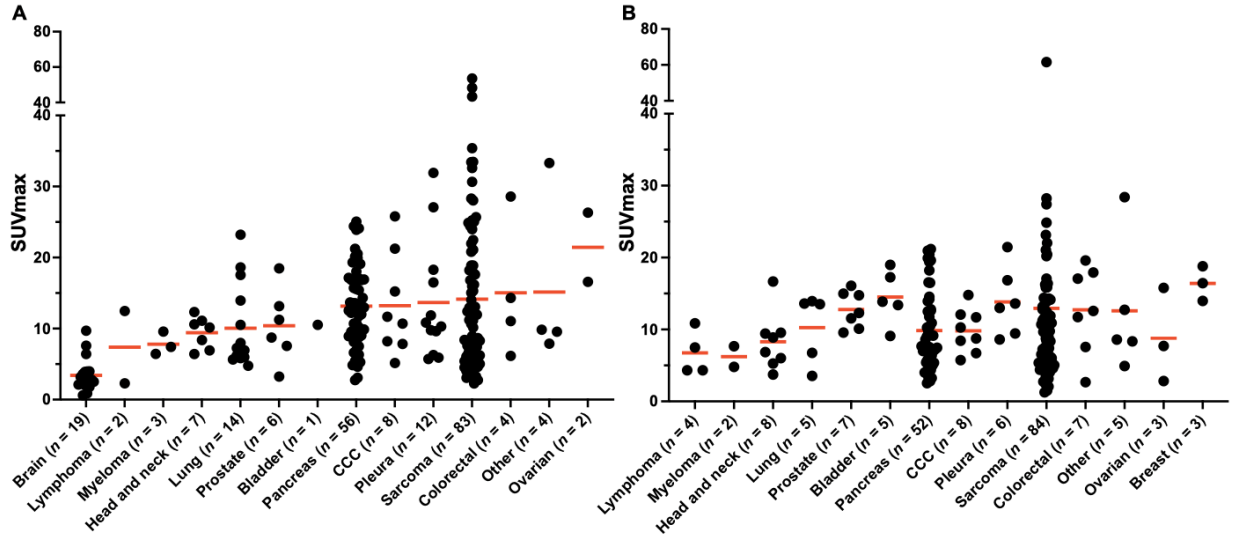

Figure 1. Mean SUV_{max} on ^{68}Ga-FAPI PET for **(A)** primary lesions (N=221) and **(B)** hottest metastatic lesions per patient (N=199). Data points represent hottest lesions for individual patients. Data in (A) and (B) were sorted by mean SUV_{max} in (A). Numbers of patients included for every tumor entity are given on the x-axis. Red lines represent mean values. Y-axis is split to account for extreme values. Primary and metastatic lesions for every tumor entity are provided in Supplemental Table 1.

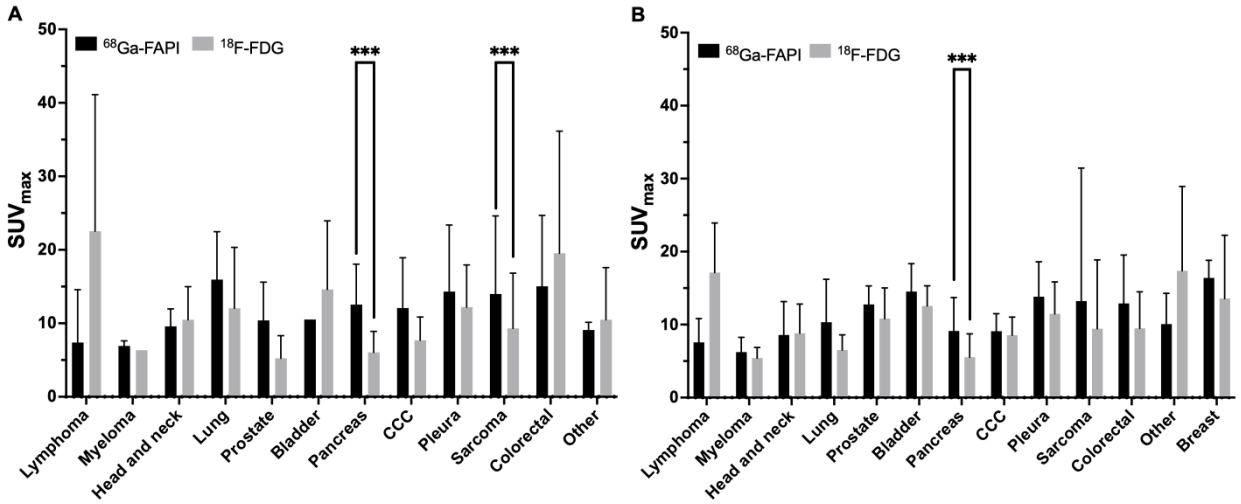

Figure 2. Comparison of mean SUV_{max} for **(A)** primary lesions and **(B)** metastatic lesions between ^{68}Ga-FAPI and ^{18}F-FDG PET across tumor entities. Entities arranged as presented in Figure 1. Mean and standard deviation are presented for every bar. Two-tailed paired t-test was performed (*p<0.05, **p<0.01, ***p<0.001).

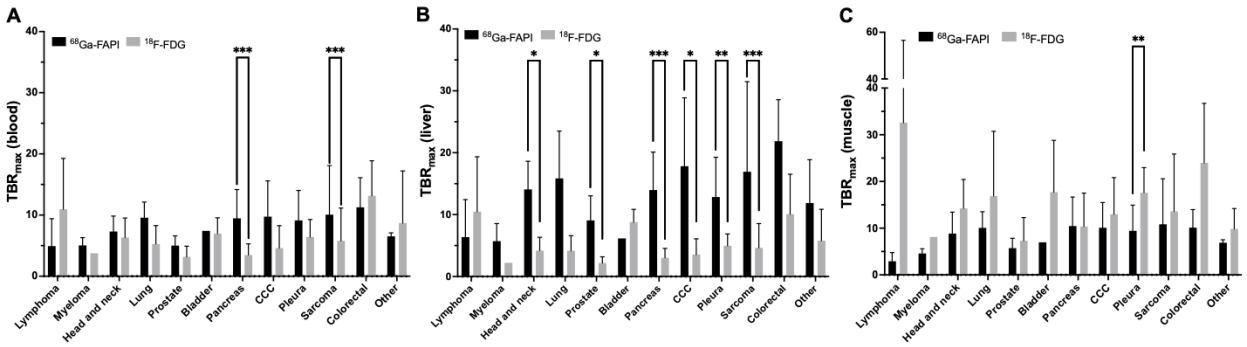

Figure 3. Comparison of mean TBR_{max} for **(A-C)** primary lesions between ^{68}Ga-FAPI and ^{18}F-FDG PET across tumor entities, with different reference backgrounds as indicated. Entities arranged as presented in Figure 1. Mean and standard deviation are presented for every bar. Two-tailed paired t-test performed (*p<0.05, **p<0.01, ***p<0.001).

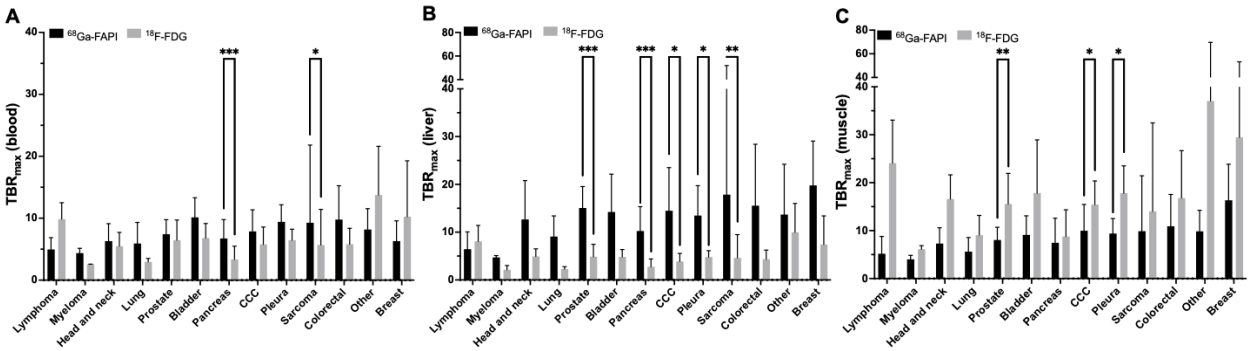

Figure 4. Comparison of mean TBR_{max} for **(A-C)** metastatic lesions between ^{68}Ga-FAPI and ^{18}F-FDG PET across tumor entities, with different reference backgrounds as indicated. Entities arranged as presented in Figure 1. Mean and standard deviation are presented for every bar. Two-tailed paired t-test performed (*p<0.05, **p<0.01, ***p<0.001).

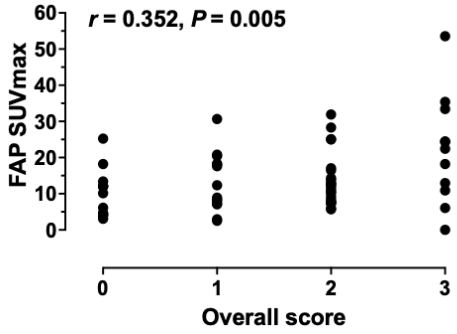

Figure 5. Correlation of ^{68}Ga-FAPI SUV_{max} with overall score for FAP-immunohistochemistry samples within 3 months from ^{68}Ga-FAPI PET (N=61). Overall FAP score refers to the highest score assigned for tumor or stroma. (r) is the Pearson correlation coefficient. Strength of correlation: negligible ($0.00 < r \leq \pm 0.29$), low ($\pm 0.30 \leq r \leq \pm 0.49$), moderate ($\pm 0.50 \leq r \leq \pm 0.69$), or high ($r \geq \pm 0.70$).

TABLES

Table 1. Patient characteristics (N=324).

Variable	N (%) or Median (IQR)
Gender	
Males	168 (52%)
Females	156 (48%)
Median age at ^{68}Ga-FAPI scan, years (IQR)	59 (16)
Tumor entities	
Sarcoma	131 (40%)
Pancreas	67 (21%)
Brain	22 (7%)
Lung	14 (4%)
Pleura	12 (4%)
Cholangiocellular	11 (3%)
Colorectal	11 (3%)
Prostate	11 (3%)
Head and neck	9 (3%)
Bladder	8 (3%)
Lymphoma	7 (2%)
Myeloma	6 (2%)
Ovarian	4 (1%)
Breast	3 (1%)
Duodenum	2 (1%)
Other*	6 (2%)
Tumor staging with ^{68}Ga-FAPI scan^{+}	
NED	19 (8%)
Stage I	26 (10%)
Stage II	29 (12%)
Stage III	25 (10%)
Stage IV	149 (60%)
Scanning purposes	
Staging at initial diagnosis	88 (27%)
Restaging after therapy	235 (73%)
Prior therapy received	
None	88 (27%)
Surgery	176 (55%)
Chemotherapy	176 (55%)
Radiation therapy	83 (26%)
Immune therapy	27 (8%)
Hormone therapy	9 (3%)
Radionuclide therapy	3 (1%)
Median uptake time, minutes (IQR)	
^{68}Ga-FAPI	14 (24)
^{18}F-FDG	67 (23)
Median time between ^{68}Ga-FAPI and ^{18}F-FDG, days (IQR)	0 (2)

*Tumors of the cervix (N=1), liver (N=1), skin (N=1), thyroid (N=1), stomach (N=1) and myoepithelial carcinoma of the knee (N=1).

$^{+}$Among the seven most common tumor entities (N=248), excluding brain tumors as well as nine sarcoma patients (not stageable according to AJCC-8).

IQR: interquartile range; NED: no evidence of disease.

Graphical Abstract

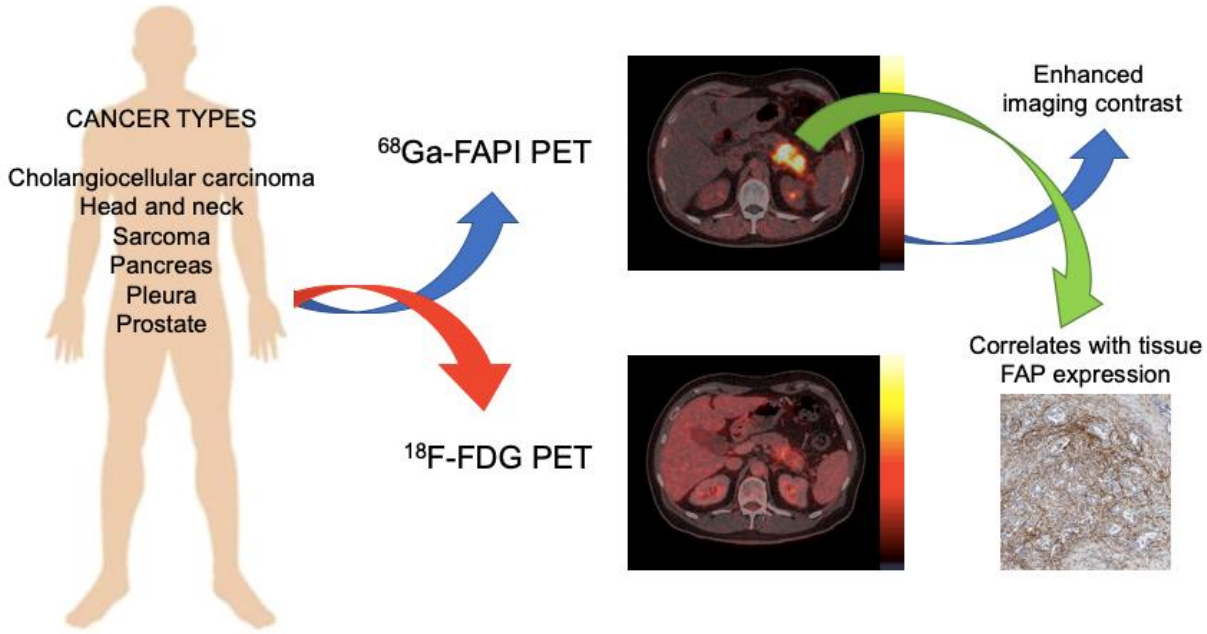

SUPPLEMENTAL TEXT

MATERIALS AND METHODS

Study design and participants

Patients underwent imaging with ^{68}Ga-FAPI PET between October 2018 and October 2021 at the Department of Nuclear Medicine at the University Hospital Essen. This is an interim analysis of the ongoing ^{68}Ga-FAPI PET observational trial conducted at the University Hospital Essen (NCT04571086). Until October 2021, adult patients who underwent clinical ^{68}Ga-FAPI PET were offered the possibility to consent to a prospective observational trial for correlation and clinical follow-up of PET findings. Evaluation of data was approved by the ethics committee of the University Duisburg-Essen (20-9485-BO and 19-8991-BO). Patient subgroups have been reported in previous publications (N=47 (*1*), N=69 (*2*), N=91 (*3*)).

Anonymized study data were managed using the Research Electronic Data Capture (REDCap) electronic data capture tools hosted at the University Hospital Essen (*4,5*). TNM staging by ^{68}Ga-FAPI PET and ^{18}F-FDG PET was determined in accordance with American Joint Committee on Cancer (AJCC) criteria, 8th edition (*6*).

PET imaging and administration of radioligand

All patients gave written informed consent to undergo a clinical ^{68}Ga-FAPI PET scan. Initially, between the period of October 2018-2019, patients received ^{68}Ga-labeled FAPI-04 ligand (N=21), and from then on, FAPI-46 has been used in our clinic and thus was received by the majority of patients in this study (N=303). Radiosynthesis and labeling were performed as described previously (*7,8*). Median injected activity of ^{68}Ga-

FAPI was 112 MBq (interquartile range (IQR): 59). PET/CT datasets for ^{68}Ga-FAPI were acquired at a median of 14 minutes after injection based on previous assessment (*2*).

^{18}F-FDG PET scans were performed as per standard of care for oncologic indications. Patients were instructed to fast for at least 6 hours before the scan to achieve serum glucose levels of <150 mg/dl prior to the scan. Median injected activity of ^{18}F-FDG was 283 MBq (IQR: 182). PET/CT datasets for ^{18}F-FDG were acquired at a median of 67 minutes after injection.

Whole body images encompassing the patients' head to mid thighs were obtained. Images were acquired using Siemens 128mCT in 52/324 cases (16%), Siemens mCT VISION in 265/324 (82%), and Siemens mMR in 7/324 (2%). All devices are cross-calibrated based on EARL accreditation standards. All PET scans were acquired in 3D mode with an acquisition time of 3 to 5 min/bed position at all sites. The median time interval between ^{18}F-FDG and ^{68}Ga-FAPI PET was 0 days (IQR: 2). For patients who underwent both ^{18}F-FDG and ^{68}Ga-FAPI PET imaging (N=237), 159/237 (67%) had received both scans on the same day (with at least 4 hours between both scans).

Imaging analysis

Each scan was analyzed on five separate levels: Primary/regional tumor, regional lymph nodes, distant lymph nodes, visceral metastases and bone metastases. Spherical volumes of interest (VOI) were used to determine maximum standardized uptake values (SUV_{max}) as well as tumor volumes of the hottest lesion at every region. A 40% isocontouring approach was used to assess metabolic tumor volume. Tracer uptake in

normal organs was quantified by SUV_{mean} using 2-cm-diameter VOIs drawn at the center of each of the aortic arch, right liver lobe, and left gluteal muscle.

Tumor-to-background ratios (TBR) were determined to quantify the image contrast. TBR_{max} was calculated by dividing the maximum SUV of the tumor by the mean SUV of the respective background (blood, liver and muscle).

Immunohistochemistry and FAP Scoring

Paraffin blocks of histopathological samples (from surgery or biopsy) dated within 3 months from the date of ^{68}Ga-FAPI PET were retrieved, such that there was no change in treatment between sampling and PET. Adequate samples were prepared and stained with FAPα antibody as described by Kessler *et al*. (*1*). Overall percentage tumor and stroma were visually quantified for every sample, and a semi-quantitative analysis for tumor and stromal FAP staining was assessed by an experienced pathologist and graded as 0 (absence or weak FAPα immunostaining in <1% of cells), 1 (focal positivity in 1-10% of cells), 2 (11-50% of cells), and 3 (51-100% staining) for tumor and stroma staining separately, as reported previously by Henry *et al*. (*9*). In addition, an overall FAP score was included for each sample using the highest score assigned for tumor and stroma scores.

Statistical analysis

Descriptive statistics were calculated. For description of SUV, arithmetic mean and standard deviation were used. After testing the data for Gaussian distribution using the Shapiro-Wilk test, comparisons of SUV and TBR between ^{68}Ga-FAPI and ^{18}F-FDG across

tumor entities were carried out with a two-tailed paired t-test. Pearson correlation coefficient was used to assess the correlation between FAPα score and the SUV_{max}, and the correlation was interpreted as negligible ($0.00 < r \leq \pm 0.29$), low ($\pm 0.30 \leq r \leq \pm 0.49$), moderate ($\pm 0.50 \leq r \leq \pm 0.69$), or high ($r \geq \pm 0.70$) (*10*). A *p*-value of <0.05 was considered statistically significant. All statistical analyses were performed using SPSS Statistics Version 28 (IBM, Armonk, NY, USA) and Excel for Mac Version 15.25 (Microsoft, Redmond, Washington, USA). GraphPad Prism for Mac version 9.3.1 (GraphPad Software, San Diego, California, USA) was used for graphical visualization.

SUPPLEMENTAL FIGURES

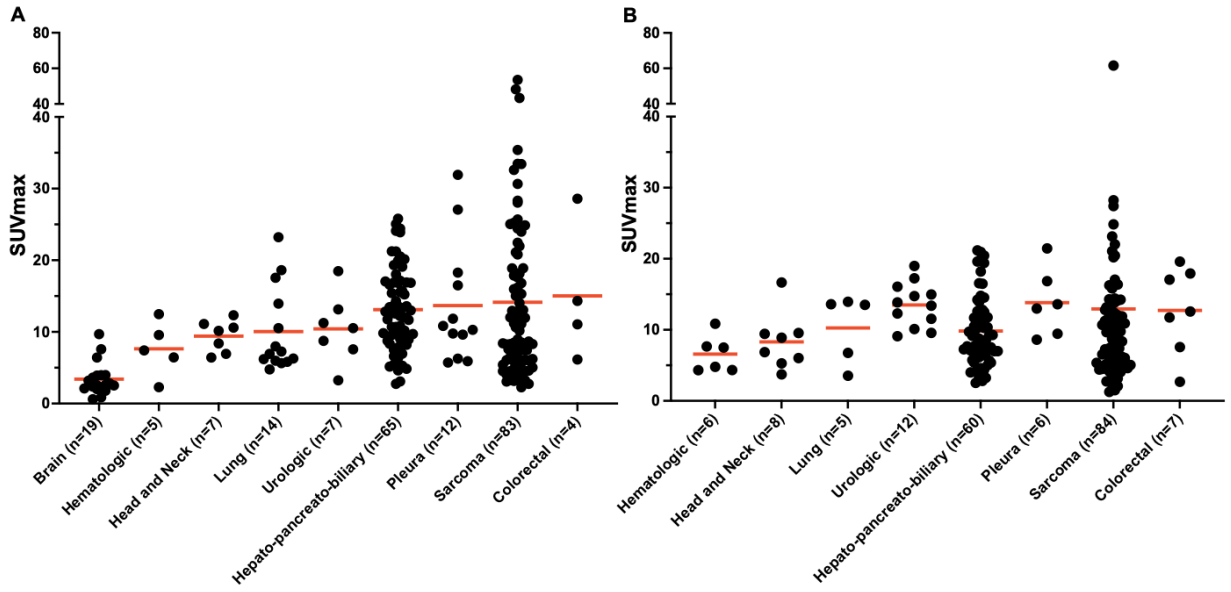

Supplemental figure 1. Mean SUV_{max} on ^{68}Ga-FAPI PET for **(A)** primary lesions (N=216) and **(B)** hottest metastatic lesions per patient (N=188) for larger subgroups (data points represent hottest lesions for individual patients). Numbers of patients included for every tumor entity are given on the x-axis. Red lines represent mean values. Y-axis is split to account for extreme values.

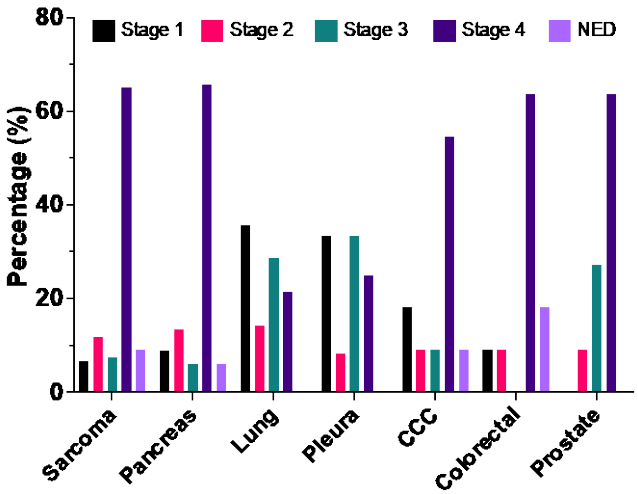

Supplemental figure 2. Staging with ^{68}Ga-FAPI PET across the seven most common tumor entities (except brain tumors and N=9 patients with sarcoma not stageable according to AJCC-8). N=248 total patients shown. M1 disease detected in majority of patients with tumors of the pancreas (44/67, 66%), sarcoma (79/122, 65%), tumors of the colon/rectum (7/11, 64%), prostate (7/11, 64%) and CCC (6/11, 55%). M0 disease detected mostly in tumors of the lung (11/14, 79%) and pleura (9/12, 75%).
CCC: cholangiocellular carcinoma; NED: no evidence of disease on ^{68}Ga-FAPI PET.

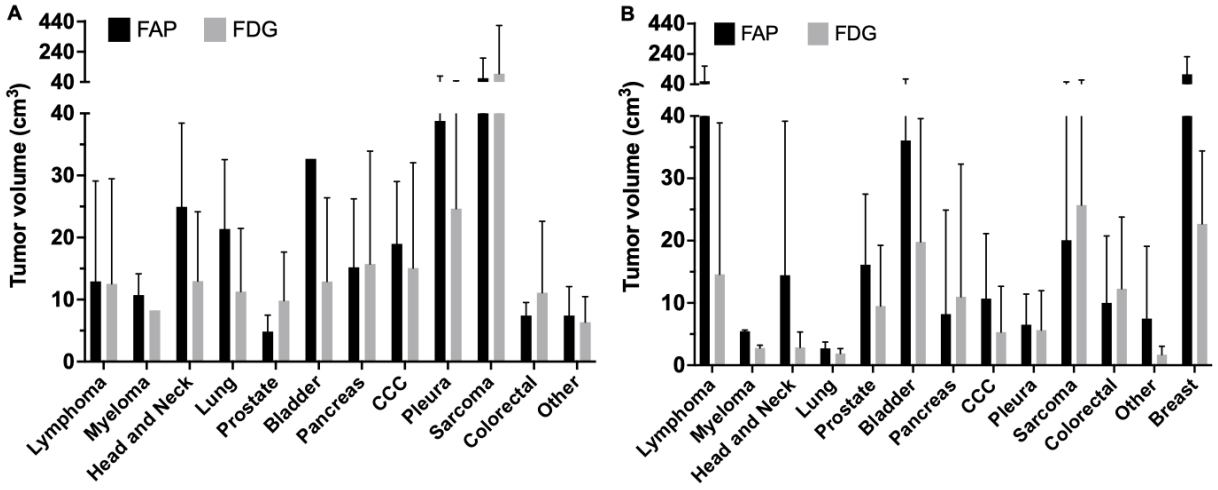

Supplemental figure 3. Comparison of tumor volumes for **(A)** primary lesions and **(B)** metastatic lesions between ^{68}Ga-FAPI and ^{18}F-FDG PET across all tumor entities. Mean and standard deviation are presented. Y-axis is split to account for extreme values.

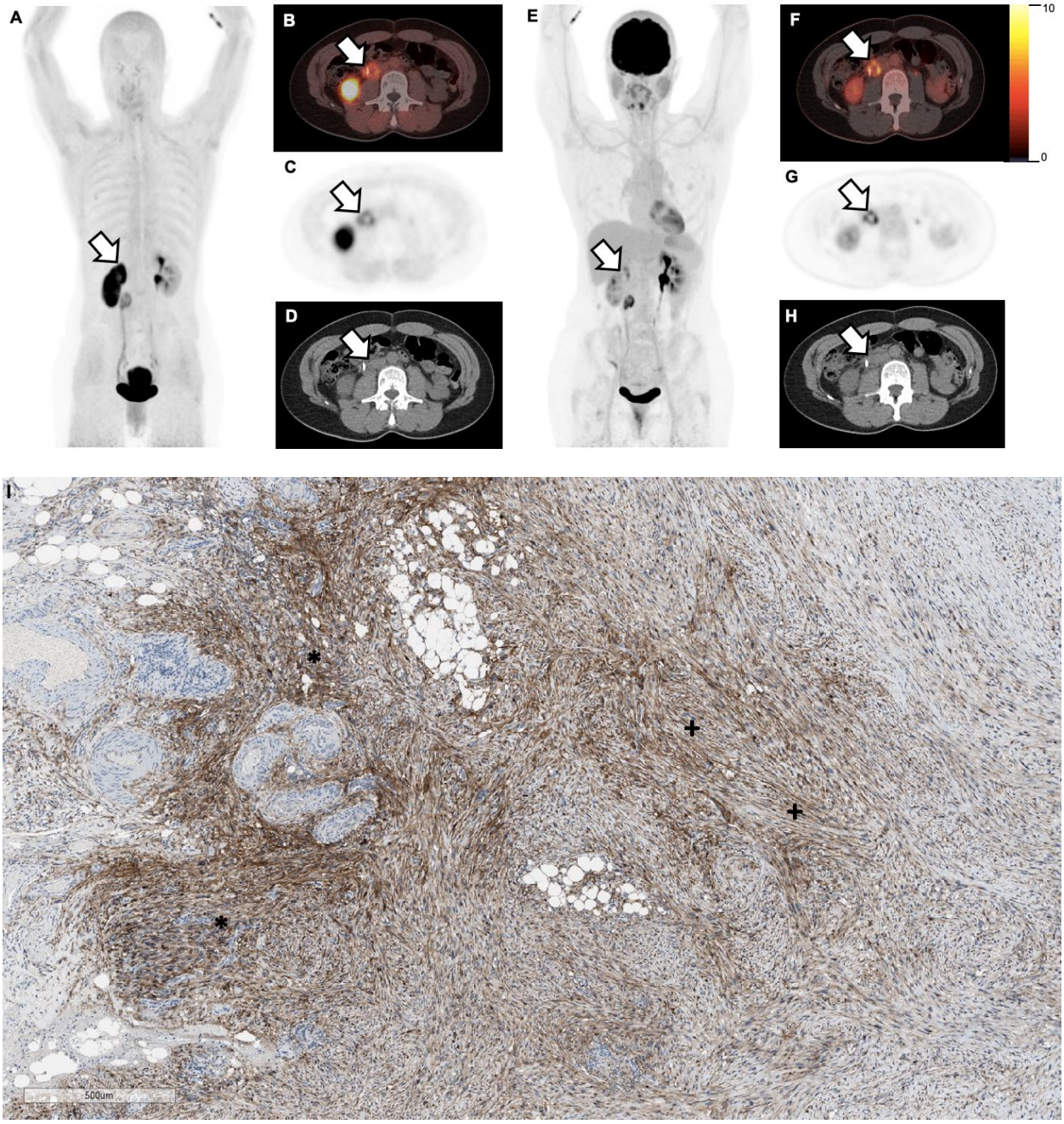

Supplemental figure 4 for a 52-year-old female with stage 2 spindle cell sarcoma (T2N0M0, G3). (A) FAPI maximum-intensity projection **(B)** fused FAPI PET/CT **(C)** FAPI PET and **(D)** accompanying low dose CT along with concomitant **(E)** FDG maximum-intensity projection **(F)** fused FDG PET/CT **(G)** FDG PET and **(H)** accompanying high dose CT. Arrows point towards visceral metastases in the right peritoneum (FAP SUVmax 6.1, FDG SUVmax 10.8). **(I)** Immunohistochemical staining with FAP antibody of a sample from the specific region reveals areas of tumor staining (>50%, score 3+; asterisks) and stromal staining (>50%, score 3+; plus sign). Overall FAP score: 3.

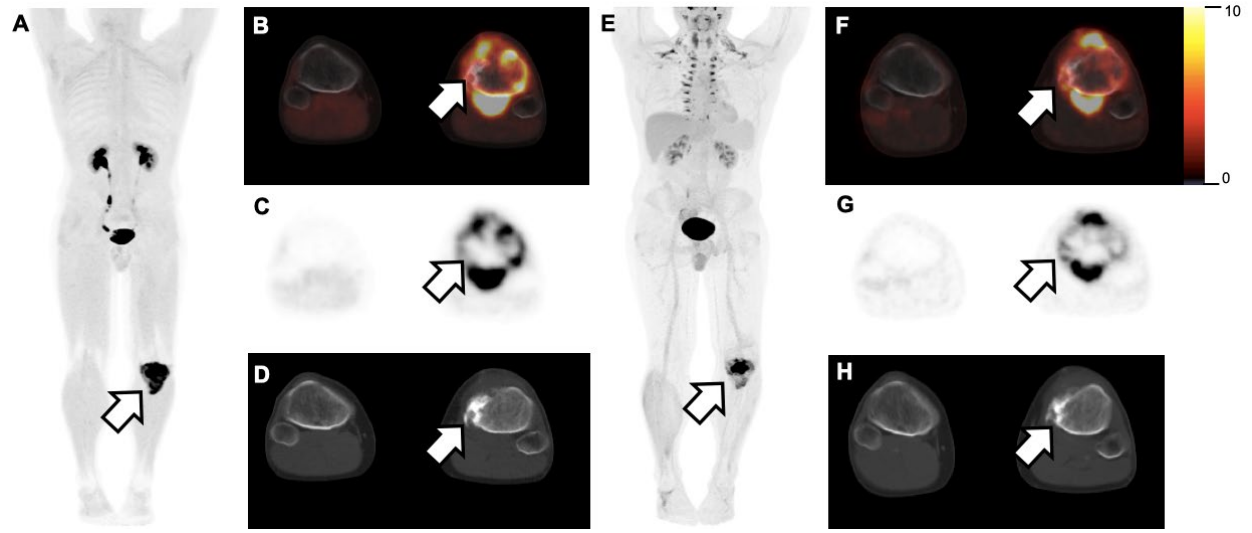

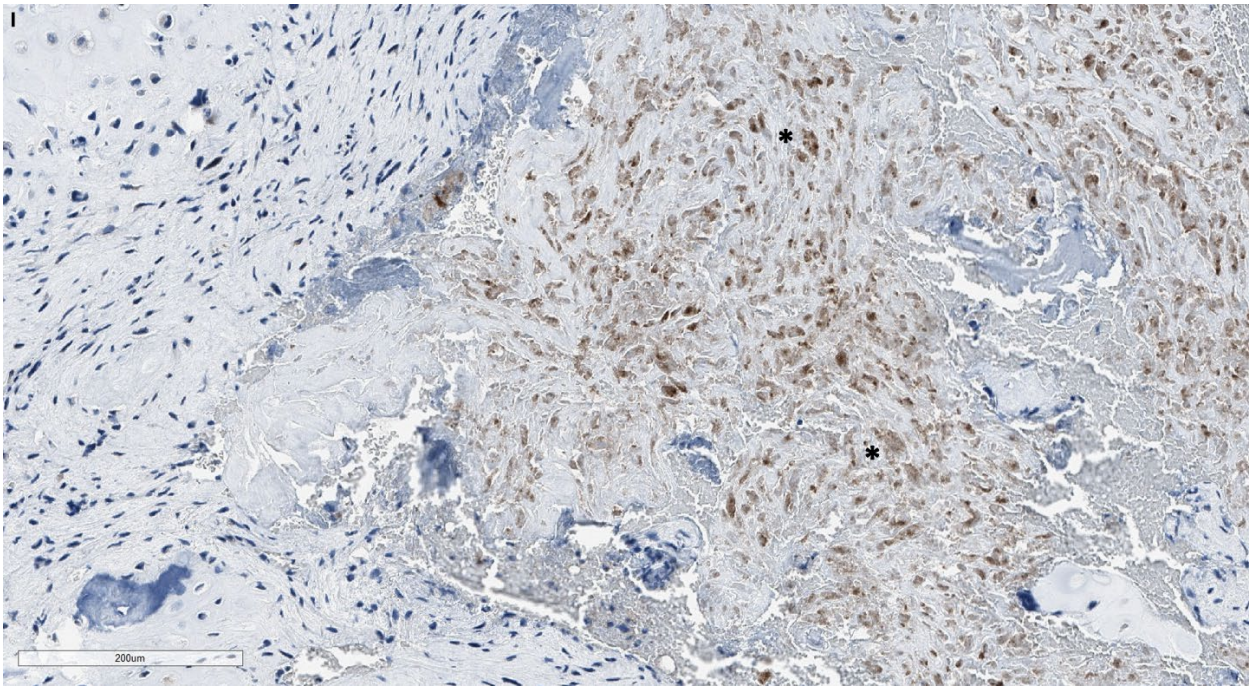

Supplemental figure 5 for a 19-year-old male with stage 2B osteosarcoma (T2N0M0, G3). **(A)** FAPI maximum-intensity projection **(B)** fused FAPI PET/CT **(C)** FAPI PET and **(D)** accompanying low dose CT along with concomitant **(E)** FDG maximum-intensity projection **(F)** fused FDG PET/CT **(G)** FDG PET and **(H)** accompanying high dose CT. Arrows point towards primary lesion in the proximal left tibia (FAP SUVmax 24.4, FDG SUVmax 18.2). **(I)** Immunohistochemical staining with FAP antibody of a sample from the specific region reveals areas of tumor staining (>50%, score 3+, asterisks). Overall FAP score: 3.

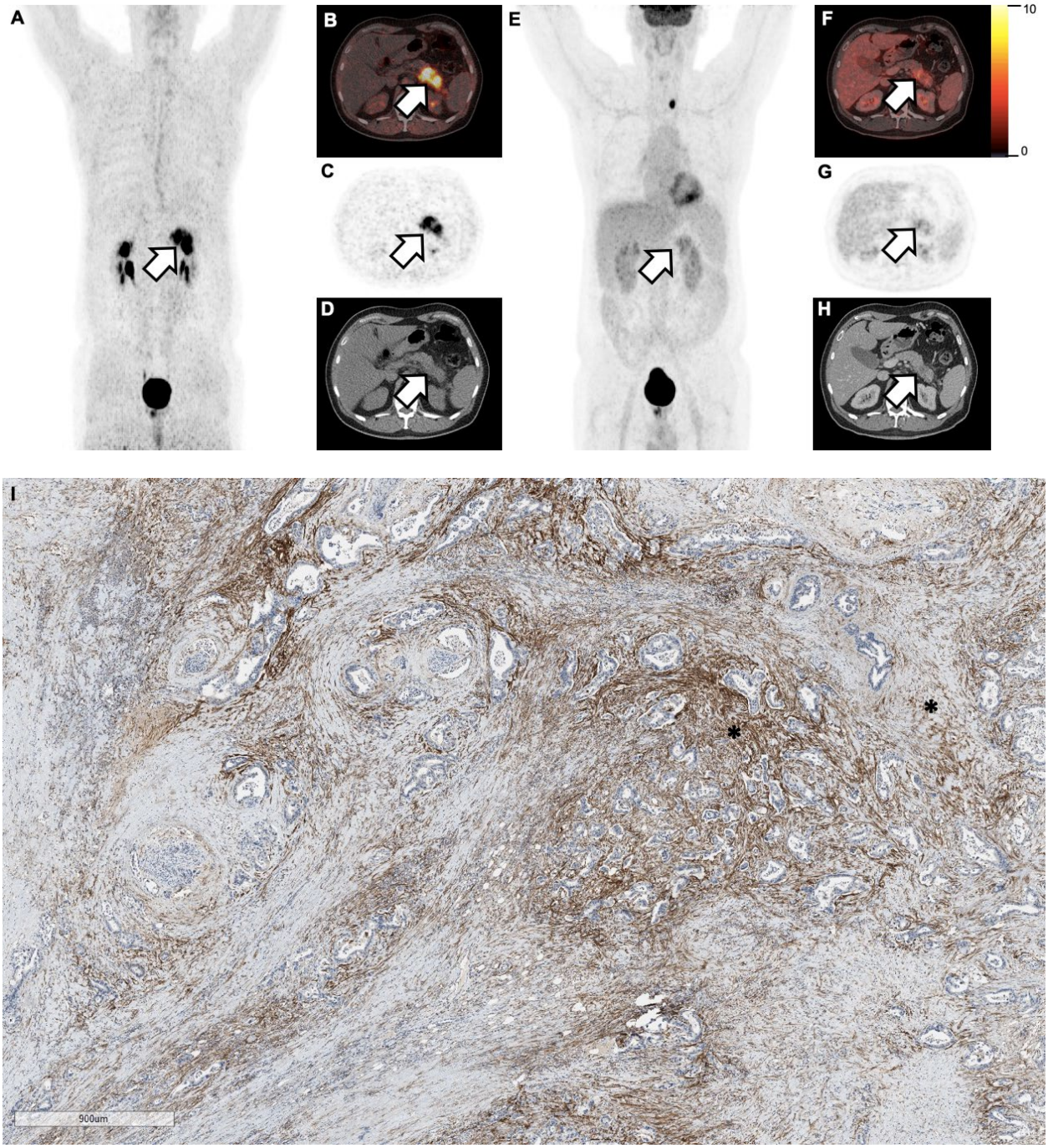

Supplemental figure 6 for a 57-year-old male with stage 1B pancreatic adenocarcinoma (T2N0M0). (A) FAPI maximum-intensity projection **(B)** fused FAPI PET/CT **(C)** FAPI PET and **(D)** accompanying low dose CT along with concomitant **(E)** FDG maximum-intensity projection **(F)** fused FDG PET/CT **(G)** FDG PET and **(H)** accompanying high dose CT. Arrows point towards primary lesion in the pancreas (FAP SUVmax 25.1, FDG SUVmax 6.2). **(I)** Immunohistochemical staining with FAP antibody of a sample from the specific region reveals areas of stromal staining (>50%, score 3+, asterisks). Overall FAP score: 3.

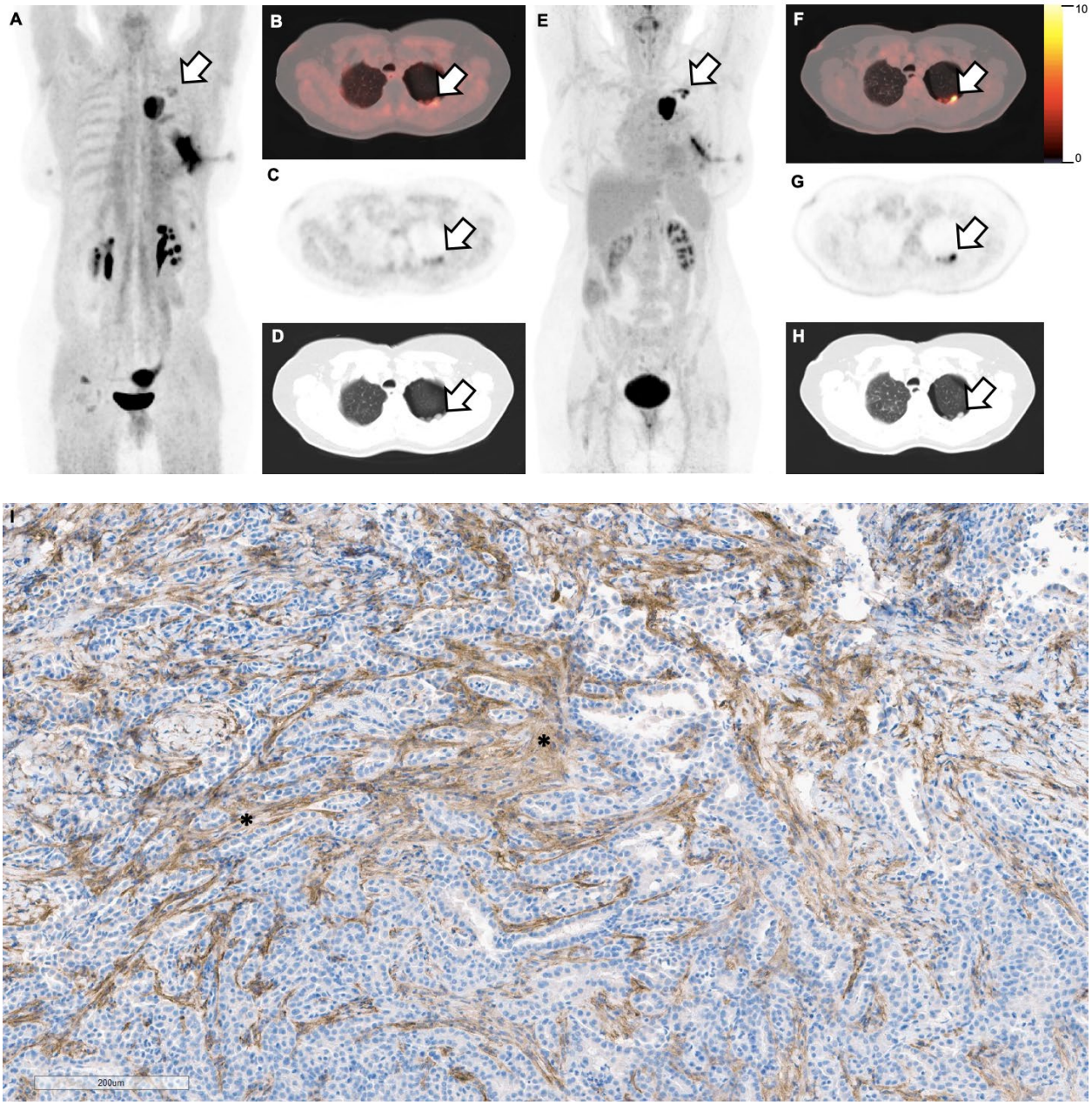

Supplemental figure 7 for a 66-year-old female with stage 2 pleural mesothelioma (T1/2N1M0). (A) FAPI maximum-intensity projection **(B)** fused FAPI PET/CT **(C)** FAPI PET and **(D)** accompanying low dose CT along with concomitant **(E)** FDG maximum-intensity projection **(F)** fused FDG PET/CT **(G)** FDG PET and **(H)** accompanying high dose CT. Arrows point towards one of the primary lesions in the left parietal dorso-apical pleura (FAP SUVmax 5.9, FDG SUVmax 11.1). **(I)** Immunohistochemical staining with FAP antibody of a sample from the specific region reveals areas of stromal staining (>50%, score 3+). Overall FAP score: 3.

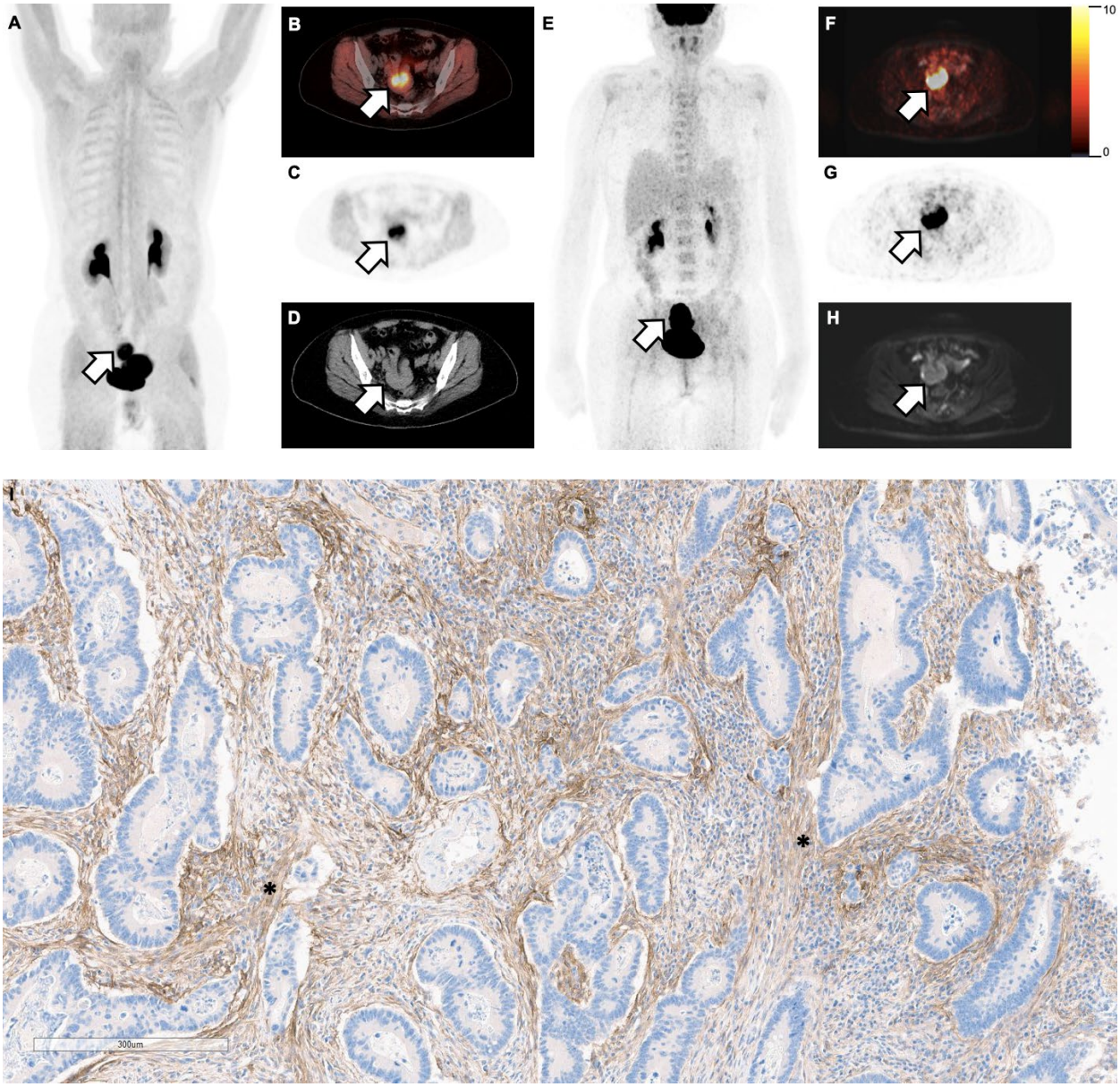

Supplemental figure 8 for a 55-year-old female with stage 2A colon adenocarcinoma (T3N0M0). (A) FAPI maximum-intensity projection **(B)** fused FAPI PET/CT **(C)** FAPI PET and **(D)** accompanying low dose CT along with concomitant **(E)** FDG maximum-intensity projection **(F)** fused FDG PET/MRI **(G)** FDG PET and **(H)** accompanying MRI. Arrows point towards the primary lesion in the left colon (FAP SUVmax 14.3, FDG SUVmax 41.3). **(I)** Immunohistochemical staining with FAP antibody of a sample from the specific region reveals areas of stromal staining (>50%, score 3+, asterisks). Overall FAP score: 3.

SUPPLEMENTAL TABLES

Supplemental Table 1. Breakdown of histopathological diagnoses as well as primary and metastatic lesions across tumor entities (N=324)

Tumor entities	Total N (% of total)	Primary lesions only, N (% of entity)	Metastatic lesions only*, N (% of entity)	Concomitant primary and metastatic lesions, N (% of entity)	NED, N (% of entity)
Sarcomas	**131 (40)**				
Angiosarcoma	2 (1)				
Chondrosarcoma	10 (3)				
Chordoma	7 (2)				
Clear cell sarcoma	3 (1)				
Endometrial sarcoma	3 (1)				
Ewing sarcoma	5 (2)				
Fibrosarcoma	11 (3)				
Gastrointestinal stromal tumors	2 (1)				
Leiomyosarcoma	9 (3)	39 (30)	40 (31)	44 (33)	8 (6)
Liposarcoma	16 (5)				
Osteosarcoma	13 (4)				
Other[+]	11 (3)				
Pleomorphic sarcoma	9 (3)				
Rhabdomyosarcoma	3 (1)				
Round cell sarcoma	2 (1)				
Solitary fibrous tumor	13 (4)				
Spindle cell sarcoma	7 (2)				
Synovial sarcoma	5 (2)				
Pancreas	**67 (21)**				
Acinar cell carcinoma	1 (0)				
Ductal adenocarcinoma	62 (19)				
Intraductal papillary mucinous neoplasia	1 (0)	14 (21)	10 (15)	42 (63)	1 (1)
Neuroendocrine carcinoma	1 (0)				
Signet ring cell carcinoma	1 (0)				
Unknown	1 (0)				
Brain	**22 (7)**				
Astrocytoma	1 (0)	19 (86)	0	0	3 (14)
Glioblastoma multiforme	19 (6)				
Unknown	2 (1)				
Lung	**14 (4)**				
Adenocarcinoma	5 (2)	9 (64)	0	5 (36)	0
Adenosquamous carcinoma	6 (2)				
Squamous cell carcinoma	3 (1)				
Pleura	**12 (4)**				
Biphasic mesothelioma	1 (0)	6 (50)	0	6 (50)	0
Epithelial mesothelioma	10 (3)				

Sarcomatoid mesothelioma	1 (0)				
Cholangiocellular carcinoma (CCC)	**11 (3)**				
Extrahepatic CCC (Klatskin tumor)	2 (1)	2 (18)	2 (18)	6 (55)	1 (9)
Extrahepatic CCC (non-Klatskin tumor)	2 (1)				
Intrahepatic CCC	7 (2)				
Colorectal	**11 (3)**				
Colon adenocarcinoma	6 (2)	2 (18)	5 (46)	2 (18)	2 (18)
Rectal adenocarcinoma	5 (2)				
Prostate	**11 (3)**	4 (36)	5 (46)	2 (18)	0
Adenocarcinoma	11 (3)				
Head and Neck	**9 (3)**				
Adenoid cystic carcinoma	5 (2)				
Polymorphic adenocarcinoma	1 (0)	1 (11)	2 (22)	6 (67)	0
Small blue round cell tumor	1 (0)				
Squamous cell carcinoma	2 (1)				
Bladder	**8 (3)**	0	4 (50)	1 (12)	3 (38)
Urothelial carcinoma	8 (3)				
Lymphoma	**7 (2)**				
NHL, diffuse large B-cell lymphoma	1 (0)	1 (14)	3 (43)	1 (14)	2 (29)
NHL, follicular lymphoma	5 (2)				
MALT lymphoma	1 (0)				
Myeloma	**6 (2)**				
IgA kappa	2 (1)				
IgG kappa	2 (1)	1 (17)	0	2 (33)	3 (50)
Light chain kappa	1 (0)				
Smouldering myeloma	1 (0)				
Ovarian	**4 (1)**				
Other	1 (0)	0	1 (25)	2 (50)	1 (25)
Serous carcinoma	3 (1)				
Breast	**3 (1)**	0	3 (100)	0	0
Tripe negative adenocarcinoma	3 (1)				
Duodenum	**2 (1)**	0	1 (50)	0	1 (50)
Duodenal adenocarcinoma	2 (1)				
Other	**6 (2)**				
Cervix, squamous cell carcinoma	1 (0)				
Knee, myoepithelial carcinoma	1 (0)				
Liver, hepatocellular carcinoma	1 (0)	2 (33)	2 (33)	2 (33)	0
Skin, melanoma	1 (0)				
Stomach, gastric adenocarcinoma	1 (0)				
Thyroid, papillary carcinoma	1 (0)				

MALT: mucosal associated lymphoid tissue; NED: no evidence of disease; NHL: non-Hodgkin's lymphoma.
* Refers to loco-regional or distant metastasis.
⁺ Each entity (N=1): Epitheloid sarcoma, follicular dendritic sarcoma, giant cell tumor, gastrointestinal neuroendocrine tumor (G-NET), hemangioendothelioma, hemangiopericytoma, myofibroblastic sarcoma, peripheral nerve sheath tumor, soft tissue sarcoma, synchronous adenosarcoma-carcinoma, vulvar sarcoma.

Supplemental Table 2. Comparison of average SUV_{max} (hottest lesion) and total number of involved regions (sum among all N=237 patients in the head-to-head comparison) between ^{68}Ga-FAPI and ^{18}F-FDG PET. Data are listed separate for non-metastatic versus distant metastatic disease by different tumor entities

	Non-metastatic (M0)				Metastatic (M1)			
	SUVmax		N involved regions		SUVmax		N involved regions	
	FAPI	FDG	FAPI	FDG	FAPI	FDG	FAPI	FDG
Lymphoma (N=6)	-	-	-	-	10.1	19.7	7	10
Myeloma (N=4)	6.9	6.3	4	3	-	-	-	-
Head and neck (N=6)	-	-	-	-	9.6	10.5	15	13
Lung (N=5)	12.8	9.4	4	4	18.6	13.4	9	8
Prostate (N=11)	7.7	3.4	4	3	15.8	7.9	20	20
Bladder (N=7)	-	19.1	-	1	10.5	7.8	8	7
Pancreas (N=41)	13.1	4.8	21	20	12.2	7.0	65	57
CCC (N=10)	17.2	6.0	5	5	8.2	9.4	12	11
Pleura (N=9)	11.0	11.6	11	11	24.2	15.0	8	8
Sarcoma (N=116)	13.7	8.9	52	48	14.3	9.7	137	131
Colorectal (N=10)	12.7	23.1	2	2	17.4	15.9	9	9
Other (N=12)	9.1	7.1	5	5	7.9	17.2	17	17

CCC: cholangiocellular carcinoma.

SUPPLEMENTAL REFERENCES

1. Kessler L, Ferdinandus J, Hirmas N, et al. (68)Ga-FAPI as a diagnostic tool in sarcoma: Data from the (68)Ga-FAPI PET prospective observational trial. *J Nucl Med.* 2022;63:89-95.

2. Ferdinandus J, Kessler L, Hirmas N, et al. Equivalent tumor detection for early and late FAPI-46 PET acquisition. *Eur J Nucl Med Mol Imaging.* 2021;48:3221-3227.

3. Kessler L, Ferdinandus J, Hirmas N, et al. Pitfalls and common findings in (68)Ga-FAPI-PET - A pictorial analysis. *J Nucl Med.* 2022;63:890-896.

4. Harris PA, Taylor R, Minor BL, et al. The REDCap consortium: Building an international community of software platform partners. *J Biomed Inform.* 2019;95:103208.

5. Harris PA, Taylor R, Thielke R, Payne J, Gonzalez N, Conde JG. Research electronic data capture (REDCap)--a metadata-driven methodology and workflow process for providing translational research informatics support. *J Biomed Inform.* 2009;42:377-381.

6. Amin MB, Edge S, Greene F, et al. *AJCC Cancer Staging Manual.* 8th ed. Springer International Publishing; 2017:55-986.

7. Lindner T, Loktev A, Giesel F, Kratochwil C, Altmann A, Haberkorn U. Targeting of activated fibroblasts for imaging and therapy. *EJNMMI Radiopharm Chem.* 2019;4:16.

8. Loktev A, Lindner T, Burger EM, et al. Development of fibroblast activation protein-targeted radiotracers with Improved tumor retention. *J Nucl Med.* 2019;60:1421-1429.

9. Henry LR, Lee HO, Lee JS, et al. Clinical implications of fibroblast activation protein in patients with colon cancer. *Clin Cancer Res.* 2007;13:1736-1741.

10. Hinkle DE, Wiersma W, Jurs SG. *Applied Statistics for the Behavioral Sciences*. 2nd ed. Boston: Houghton Mifflin; 2003: 118.